Progress In Electromagnetics Research, PIER 69, 161–176, 2007

THE MULTILEVEL FAST MULTIPOLE ALGORITHM FOR EMC ANALYSIS OF MULTIPLE ANTENNAS ON ELECTRICALLY LARGE PLATFORMS

X. W. Zhao, X. J. Dang, Y. Zhang, and C. H. Liang

National Key Laboratory of Antennas and Microwave Technology
Xidian University
Xi'an, Shaanxi 710071, China

Abstract—The new definition of arbitrary isolation between antennas is proposed according to the microwave network theory. The multilevel fast multipole algorithm (MLFMA) with the near-field preconditioner is implemented to predict the isolation between multiple antennas on electrically large platforms over a wide frequency range. Experimental results show that the isolation defined in this paper is more practical than the traditional one. Finally the radiation pattern and the isolation results for the ultra-shortwave antennas mounted on full-scale models such as an aircraft and a ship are obtained and discussed, which can give significant instructions to the platform-mounted antennas design.

1. INTRODUCTION

On electrically large platforms (such as aircrafts and ships), more and more antennas are used for different purposes, which will suffer more electromagnetic interference (EMI) problems than before. On the other hand, the platforms also degrade the performance of these platform-mounted antennas. Therefore, it has become increasingly important to simulate and analyze the electromagnetic compatibility (EMC) problems including multiple platform-mounted antennas.

In EMC study, the interaction of two-antenna system is usually described with the isolation between antennas. The isolation is traditionally defined as $10\lg\left(1/\left|S_{21}\right|^2\right)$ [1]. Our previous research [2] points out that the isolation value calculated with the traditional formula is usually optimistically better than the actual one, therefore it may give the error message that the two antennas are well isolated.

On the other hand, there are lots of commercial EM softwares available, such as Ansoft and NEC. However, most of them can not deal

with large-scale EM problems. As is well known, the multilevel fast multipole algorithm (MLFMA) is one of the most efficient approaches to solve the integral equation relevant to electromagnetic radiation and scattering problems [3–5]. In the MLFMA, both the computational and memory complexities for a matrix-vector product are reduced from $O(N^2)$ to $O(N \log N)$ [6, 7], where N is the number of unknowns. The low complexity of the MLFMA is especially favorable for fast solving large-scale EMC problems over a sweep of frequencies [8]. Unfortunately, even if some softwares such as FEKO utilize the MLFMA, however, most of these softwares can not obtain the isolation between antennas directly.

To simulate real engineering problems, in this paper, the authors will put forward the definition of arbitrary isolation between antennas according to the microwave network theory with the reciprocity theorem considered. The MLFMA with adaptive number of levels is implemented to predict the arbitrary isolation between antennas on electrically large platforms. Furthermore, based on our previous research [9–11], an efficient near-field preconditioner is combined with BiCGStab(l) as the solver to improve greatly the efficiency of the MLFMA [12, 13]. Experimental results are achieved to validate the formula and the algorithm. The radiation pattern and the isolation results including airborne and shipborne antennas are obtained and discussed, and these results can give significant instructions to the platform-mounted antennas design.

2. BASIC THEORY FOR INTERCONNECTED SYSTEM

2.1. Fundamental Knowledge of Basis Functions and MLFMA

Consider a perfect electric conductor (PEC) S consisting of surfaces, wires, and surface-wire junctions. Applying the boundary condition on the PEC surface, we obtain the electric field integral equation (EFIE) as

$$\hat{\boldsymbol{t}} \cdot \int_S \overline{\boldsymbol{G}}\left(\boldsymbol{r}, \boldsymbol{r}'\right) \cdot \boldsymbol{J}\left(\boldsymbol{r}'\right) dS' = \frac{4\pi i}{k\eta} \hat{\boldsymbol{t}} \cdot \boldsymbol{E}^i\left(\boldsymbol{r}\right) \tag{1}$$

where $\overline{\boldsymbol{G}}\left(\boldsymbol{r}, \boldsymbol{r}'\right)$ is the free space Green's function, $\boldsymbol{E}^i\left(\boldsymbol{r}\right)$ is the incident electric field, $\boldsymbol{J}\left(\boldsymbol{r}'\right)$ is the unknown current density, k is the free space wavenumber and η is the free space wave impedance.

As depicted in Fig. 1, RWG basis functions $\boldsymbol{j}_n^B$ are chosen to expand the unknown surface current density, pulse basis functions $\boldsymbol{j}_n^W$ are chosen to expand the unknown wire current and Costa basis functions $\boldsymbol{j}_n^J$ are chosen to expand the unknown surface-wire junction

current [14]. Costa basis functions preserve the continuity of currents over discretized triangular patches and linear segments, thus enabling the application of the MoM/MLFMA to the analysis of electromagnetic phenomena involving complex metallic structures.

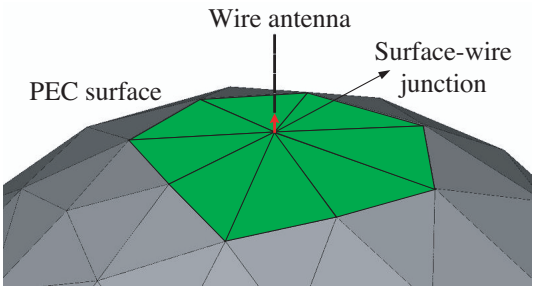

Figure 1. Surface-wire structure.

The current distribution $\boldsymbol{J}(\boldsymbol{r}')$, can be expressed as a linear superposition of body surface (B), wire (W), and junction (J) basis functions, respectively,

$$\boldsymbol{J} = \sum_{n=1}^{N_B} I_n^B \boldsymbol{j}_n^B(\boldsymbol{r}') + \sum_{n=1}^{N_W} I_n^W \boldsymbol{j}_n^W(\boldsymbol{r}') + \sum_{n=1}^{N_J} I_n^J \boldsymbol{j}_n^J(\boldsymbol{r}') \tag{2}$$

Applying Galerkin's method, one can express the interaction of the current on different basis functions as an impedance matrix and solve for the unknown current using the matrix equation

$$\begin{bmatrix} \boldsymbol{Z}^{BB} & \boldsymbol{Z}^{BW} & \boldsymbol{Z}^{BJ} \\ \boldsymbol{Z}^{WB} & \boldsymbol{Z}^{WW} & \boldsymbol{Z}^{WJ} \\ \boldsymbol{Z}^{JB} & \boldsymbol{Z}^{JW} & \boldsymbol{Z}^{JJ} \end{bmatrix} \begin{bmatrix} \boldsymbol{I}_B \\ \boldsymbol{I}_W \\ \boldsymbol{I}_J \end{bmatrix} \begin{bmatrix} \boldsymbol{V}_B \\ \boldsymbol{V}_W \\ \boldsymbol{V}_J \end{bmatrix} \tag{3}$$

The entries in the impedance matrix and the source vector are given by

$$Z_{ji} = \int_S dS\, \boldsymbol{t}_j(\boldsymbol{r}) \cdot \int_S dS' \overline{\boldsymbol{G}}(\boldsymbol{r}, \boldsymbol{r}') \cdot \boldsymbol{j}_i(\boldsymbol{r}') \tag{4}$$

$$V_j = \frac{4\pi i}{k\eta} \int_S dS\, \boldsymbol{t}_j(\boldsymbol{r}) \cdot \boldsymbol{E}^i(\boldsymbol{r}) \tag{5}$$

where $\boldsymbol{j}_i$ and $\boldsymbol{t}_j$ are the basis functions and the testing functions, respectively ($\boldsymbol{j}_i$ and $\boldsymbol{t}_j$ can be replaced by $\boldsymbol{j}_n^B$, $\boldsymbol{j}_n^W$ and $\boldsymbol{j}_n^J$).

The fast multipole method (FMM) is based on the fact that the number of interactions described by a classical MoM matrix can be

reduced by grouping current basis functions together. Suppose that the field (observation) point $\boldsymbol{r}_j$ belongs to a group with $\boldsymbol{r}_m$ as the group center, and the source point $\boldsymbol{r}_i$ belongs to a group with $\boldsymbol{r}_{m'}$ as the group center. If the distance between the group centers is larger than the group size, the matrix element Z_{ji} can be written as

$$Z_{ji} = \frac{ik}{4\pi} \int d^2\hat{\boldsymbol{k}} \boldsymbol{V}_{fmj}\left(\hat{\boldsymbol{k}}\right) \cdot \alpha_{mm'}\left(\hat{\boldsymbol{k}} \cdot \hat{\boldsymbol{r}}_{mm'}\right) \cdot \boldsymbol{V}^*_{sm'i}\left(\hat{\boldsymbol{k}}\right) \quad (6)$$

$$\boldsymbol{V}_{sm'i}\left(\hat{\boldsymbol{k}}\right) = \left[\overline{\boldsymbol{I}} - \hat{\boldsymbol{k}}\hat{\boldsymbol{k}}\right] \cdot \int_S dS' \boldsymbol{j}_i\left(\boldsymbol{r}_{im'}\right) e^{ik \cdot r_{im'}} \quad (7)$$

$$\boldsymbol{V}_{fmj}\left(\hat{\boldsymbol{k}}\right) = \left[\overline{\boldsymbol{I}} - \hat{\boldsymbol{k}}\hat{\boldsymbol{k}}\right] \cdot \int_S dS\, \boldsymbol{t}_j\left(\boldsymbol{r}_{jm}\right) e^{ik \cdot r_{jm}} \quad (8)$$

$$\alpha_{mm'}\left(\hat{\boldsymbol{r}}_{mm'} \cdot \hat{\boldsymbol{k}}\right) = \sum_{l=0}^{L} i^l (2l+1) h_l^{(1)}\left(kr_{mm'}\right) P_l\left(\hat{\boldsymbol{r}}_{mm'} \cdot \hat{\boldsymbol{k}}\right) \quad (9)$$

where $\boldsymbol{V}_{sm'i}$ is the radiation pattern of a source point, $\boldsymbol{V}_{fmj}$ is the receiving pattern of a field point, and the precomputed translation matrix $\bar{\boldsymbol{\alpha}}$ translates the field from the source to the receiving group. By choosing a plane wave expansion as the basis to the Green's function, the translation matrix is inherently diagonal. Thus, the amount of computation involved in evaluating (6) is greatly reduced. However, when the source point and the field point fall within adjacent groups, their interaction should be evaluated by (4). The overall complexity of computing the matrix-vector multiplication is $O(N^{1.5})$ per iteration for this simple two-level scheme. Comparing with the complexity of applying an iterative solver directly to a classical MoM matrix, which is $O(N^2)$, the FMM obviously is more efficient. The idea of grouping basis functions can be extended to the idea of collecting group centers and forming a multilevel tree structure. By applying the grouping process repeatedly, we can form the multilevel FMM with a complexity of $O(N \log N)$ per iteration.

The MLFMA first encloses the scatter in a large cube of edge length D, and then this cube (or any subcube) is recursively divided into eight smaller cubes until the edge length $d_g = D/2^g$ at the finest level g is approximately half a wavelength. Here we use $d_g = \xi \cdot 2\pi/|k|$ with ξ in the range $0.25 \leq \xi \leq 0.6$, i.e., the adaptive number of MLFMA levels is given by

$$g = \mathrm{NINT}\left[\ln\left(\frac{D\,|k|}{2\pi\xi}\right) \Big/ \ln 2\right] \quad (10)$$

where NINT$(\cdot)$ denotes the closest integer (next integer) value.

2.2. Near-field Preconditioner

A near-field preconditioner is physical-based, and takes the contribution of the most important part of near field [9–11]. It is effective in accelerating convergence of surface, volume, and combined surface/volume integral equations for a broad variety of electromagnetic scattering problems. A BiCGstab(l) iterative solver in conjunction with the near-field preconditioner can significantly reduce the number of iterations required for convergence [12, 13]. The detailed procedure of the near-field preconditioning scheme is as following [9]:

Let $\boldsymbol{P}$ be the preconditioner matrix. For the ith row $\boldsymbol{p}_i$ of $\boldsymbol{P}$:

(1) Let a list $L_i = \left\{\boldsymbol{j}_i^{(1)}, \boldsymbol{j}_i^{(2)}, \cdots, \boldsymbol{j}_i^{(K)}\right\}$ contain all the testing functions within a prescribed distance R_p of the ith basis function $\boldsymbol{j}_i$.

(2) Solve the small system $\bar{\boldsymbol{Z}}^T \bar{\boldsymbol{p}}_i = \bar{\boldsymbol{e}}_i$, where the bars over the variables indicate that all the rows and columns except for those in the list L_i are deleted, and $\boldsymbol{e}_i$ is the ith column of the identity matrix.

(3) Scatter the entries of the solution vector $\bar{\boldsymbol{p}}_i$ back to their original coordinate position in $\boldsymbol{p}_i$, and fill the remaining positions of $\boldsymbol{p}_i$ with zero.

The rows of $\boldsymbol{P}$ are generated independently and can be done in parallel. In practice, we search the needed elements from $\boldsymbol{Z}^{near}$ and fill them in $\bar{\boldsymbol{Z}}$. Careful inspection of the procedure above reveals that N inversions of the local impedance matrices $\bar{\boldsymbol{Z}}^T$ are required to compute the complete preconditioner. The dimension of $\bar{\boldsymbol{Z}}^T$ typically is very small, and therefore the computation of $\boldsymbol{P}$ is of $O(N)$ complexity. Note that $\boldsymbol{P}$ can be very sparse, and we only need store the approximately NK nonzero elements in $\boldsymbol{P}$.

In this paper, the distance R_p is chosen as 0.125λ in the surface region and 0.5λ in the wire and junction regions, where λ is the free space wavelength.

3. ARBITRARY ISOLATION BETWEEN ANTENNAS

The isolation between antennas is an important index in electromagnetic compatibility (EMC). As shown in Fig. 2, there is an arbitrary two-antenna system. The two-antenna system can be equivalent to a two-port network, with the transmitter and the receiver regarded as the source and the load, respectively, as illustrated in Fig. 3. With the reciprocity theorem considered, the network is analyzed by employing the microwave network theory [15].

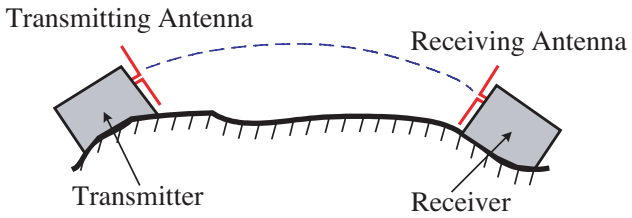

Figure 2. Arbitrary two-antenna system.

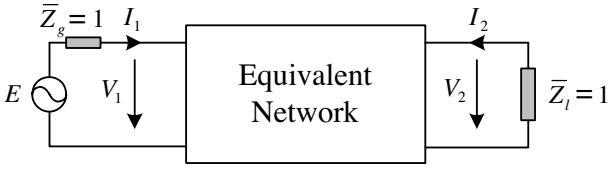

Figure 3. Equivalent network to system in Fig. 2.

The traditional isolation formula is $10\lg\left(1/|S_{21}|^2\right)$ [1]. $1/|S_{21}|^2$ is equal to the ratio of P_a to P_l, where P_a and P_l are the available power of the transmitter and the absorbed power of the receiver, respectively. P_a is determined by the transmitter and is not directly related to antenna system, therefore it can not describe the EMC characteristics of antenna system exactly. Furthermore, since P_a is the maximum power that the transmitter can provide, the isolation value calculated with the traditional formula is usually optimistically better than the actual one [2]. Note that the "ideal isolation" and "practical isolation" equations in [2] only hold for the case of weak coupling antennas. Since the traditional definition of isolation is unreasonable, it is necessary to explore new theoretic analysis of isolation between antennas.

When the source and the load are both matched, i.e., $\bar{Z}_g = \bar{Z}_l = \bar{Z}_0 = 1$, the arbitrary isolation between antennas is defined as

$$I_A = 10\lg\left(P_i/P_l\right) \tag{11}$$

where P_i is the input power of the equivalent network and P_l is the absorbed power of the load. P_i and P_l are given as

$$P_i = \frac{1}{2}\mathrm{Re}\left(V_1 I_1^*\right) \qquad P_l = \frac{1}{2}\mathrm{Re}\left(-V_2 I_2^*\right) \tag{12}$$

Based on the two-port configuration of Fig. 3, we have that

$$\begin{cases} V_1 = \bar{Z}_{11} I_1 + \bar{Z}_{12} I_2 \\ V_2 = \bar{Z}_{12} I_1 + \bar{Z}_{22} I_2 \end{cases} \tag{13}$$

where the reciprocity is considered, i.e., $\bar{Z}_{21} = \bar{Z}_{12}$.

The normalized input impedance at port one is

$$\bar{Z}_{in} = \frac{V_1}{I_1} = \bar{Z}_{11} - \frac{\bar{Z}_{12}^2}{\bar{Z}_{22} + \bar{Z}_l} \tag{14}$$

The input power P_i at port one can be written as

$$P_i = \frac{1}{2}\mathrm{Re}\left(|I_1|^2 \bar{Z}_{in}\right) = \frac{1}{2}|I_1|^2 \,\mathrm{Re}\left(\bar{Z}_{11} - \frac{\bar{Z}_{12}^2}{\bar{Z}_{22} + 1}\right) \tag{15}$$

where $\bar{Z}_l = 1$ has been considered.

Substituting $V_2 = -I_2 \bar{Z}_l = -I_2$ into the second formula of (13) yields

$$I_2 = -\frac{\bar{Z}_{12}}{\bar{Z}_{22} + 1} I_1 \tag{16}$$

$$V_2 = -I_2 \bar{Z}_l = \frac{\bar{Z}_{12}}{\bar{Z}_{22} + 1} I_1 \tag{17}$$

The absorbed power of the load P_l can be written as

$$P_l = \frac{1}{2}\mathrm{Re}\left(-V_2 I_2^*\right) = \frac{1}{2}|I_1|^2 \left|\frac{\bar{Z}_{12}}{\bar{Z}_{22} + 1}\right|^2 \tag{18}$$

Substituting (15) and (18) into (11) gives the arbitrary isolation between antennas as

$$I_A = 10 \lg \frac{\mathrm{Re}\left(\bar{Z}_{11} - \dfrac{\bar{Z}_{12}^2}{\bar{Z}_{22} + 1}\right)}{\left|\dfrac{\bar{Z}_{12}}{\bar{Z}_{22} + 1}\right|^2} \tag{19}$$

For weak coupling antennas, $\bar{Z}_{12}$ is the first-order small quantity, therefore the approximate expression of I_A is

$$I_A \approx -20 \lg \left|\bar{Z}_{12}\right| + 20 \lg \left|1 + \bar{Z}_{22}\right| + 10 \lg \left[\mathrm{Re}\left(\bar{Z}_{11}\right)\right] \tag{20}$$

Actually, Eq. (20) is a effective estimation to the isolation.

4. NUMERICAL RESULTS AND DISCUSSION

In this section, the typical model, i.e., the cylinder-mounted antennas, will be analyzed first to validate the isolation theory and the algorithm. Following that, two actual examples including airborne and shipborne antennas are considered.

The algorithm code of this work is written in Fortran 90 format (double precision) and run on a single PC (Pentium IV 2.8 GHz CPU, 2.0 GBytes Memory). The models in this section are built with Rhinoceros software and meshed with FEMAP software. The system impedance in computation and in measurement is both 50 Ω.

4.1. Example I: Validation of Isolation Theory and Code Developed

To demonstrate the accuracy and applicability of the present method, the radiation pattern and the isolation results for two cylinder-mounted antennas are calculated and compared with the experimental results. As shown in Fig. 4, the radius of the PEC cylinder is 0.19 m, and the height is 0.5 m. Two 400-MHz $\lambda/4$ monopoles are mounted on the cylinder, and in the x and y directions, respectively. The coordinates of the two joints are (0.19,0.,0.25) and (0.,0.19,0.25), respectively. The cylinder surface is meshed into 2778 planar triangles (about 30 edges/wavelength at the center frequency), and each antenna is divided into 22 segments. The isolation is computed over a frequency range of 200 MHz∼800 MHz (31 sampling points). The experimental model

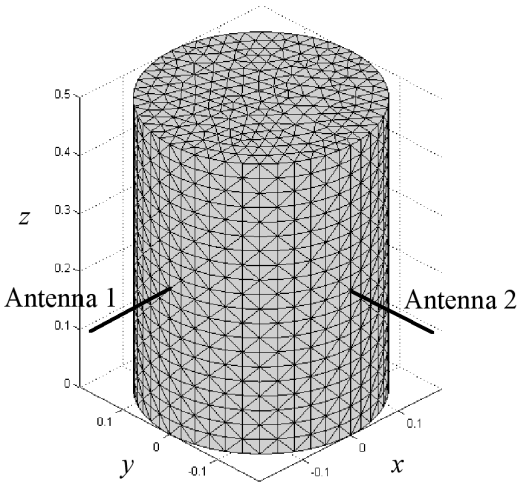

Figure 4. Two monopole antennas on a PEC cylinder.

is depicted in Fig. 5. **Note that**, both antennas in measurement are identical; the external physical structures of the antennas are radome, and the internal are just the (wide-band) 400-MHz $\lambda/4$ monopoles for aircraft communications. The radome of the antennas is designed according to the principle of aerodynamics.

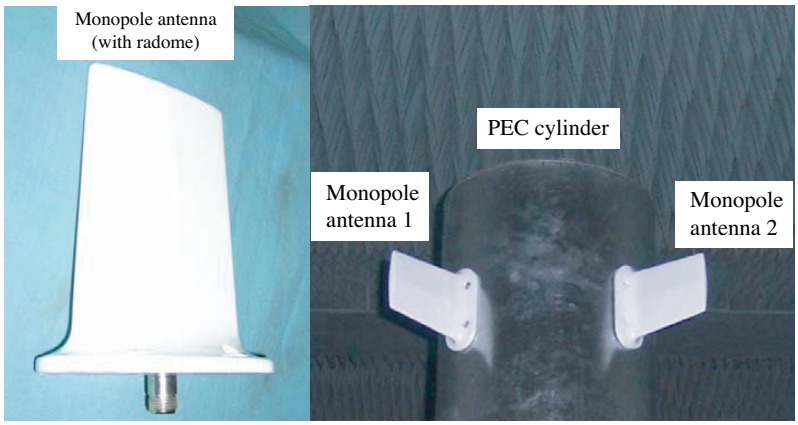

Figure 5. Experimental model for Fig. 4.

Both monopoles are joint-fed by point generators of equal amplitudes and phases. The radiation pattern of the antennas at 400 MHz is given in Fig. 6. It is obvious that the MLFMA computed results agree very well with the measured ones.

The isolation between the two antennas is given in Fig. 7. The voltage standing wave ratio (VSWR) in the input and output ports of the network are considered both in the computation and measurement, while the VSWR is not included in the arbitrary isolation in [2]. From comparison, it can be seen that the result of the arbitrary isolation defined in this paper is consistent with the measured one, which validates the correctness of the formula and the algorithm. Moreover, it is clearly shown that the traditional isolation result is higher than the measured result over the frequency range, which conforms to the theoretical analysis in Section 3.

As is well known, the classical MoM is prohibitively expensive in both memory and CPU time as the frequency increases. Thus, given the limited resource of computer memory, the MLFMA is the favorable algorithm for analyzing an object of large electrical size. Two real-world instances of large electrical size are given below.

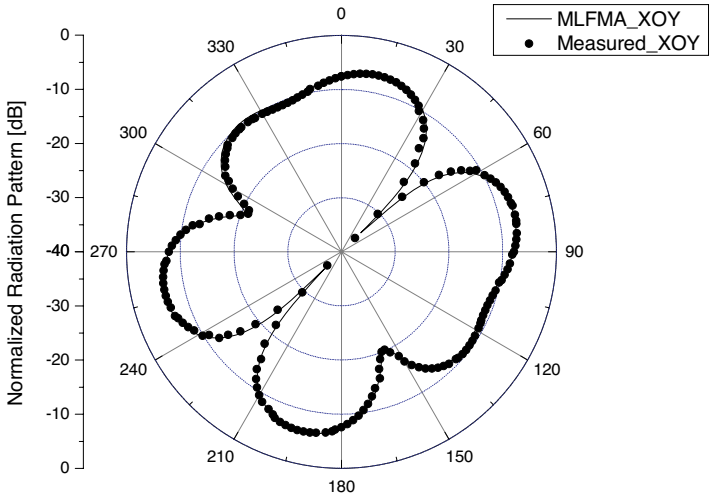

(*a*) *xoy*-plane

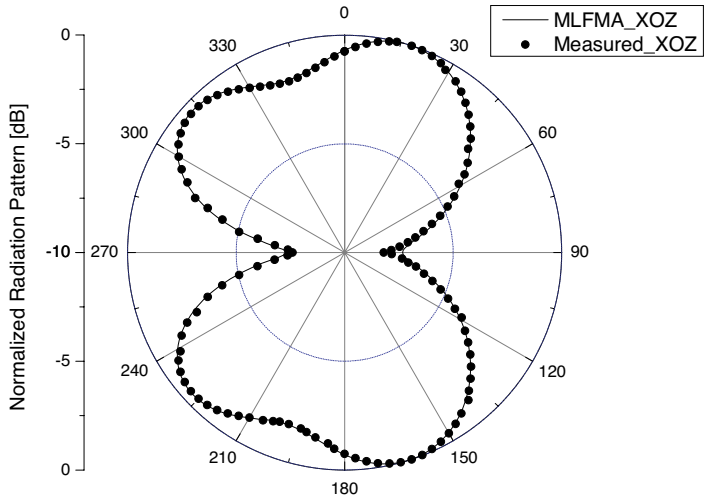

(*b*) *xoz*-plane

Figure 6. Normalized radiation pattern of cylinder-mounted antennas.

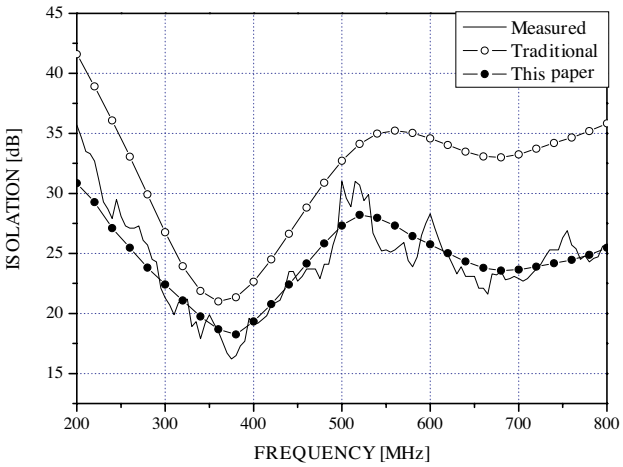

Figure 7. Isolation between cylinder-mounted antennas.

4.2. Example II: Airborne Monopole Antennas

This example applies the MLFMA to the EMC analysis of multiple antennas mounted on an electrically large platform — a Boeing 747 aircraft. The fuselage is 70.7 m long, and the wingspan is 64.4 m. Three thin-wire monopole antennas are positioned on the model as shown in Fig. 8. Each monopole is 1.5 m in length. The surface of the aircraft is represented by 15704 planar triangles (about 10 edges/wavelength at 50 MHz), and each antenna is divided into 12 segments. The center frequency of the antennas is 50 MHz, and the isolation is computed over a frequency range of 30 MHz∼70 MHz (41 sampling points).

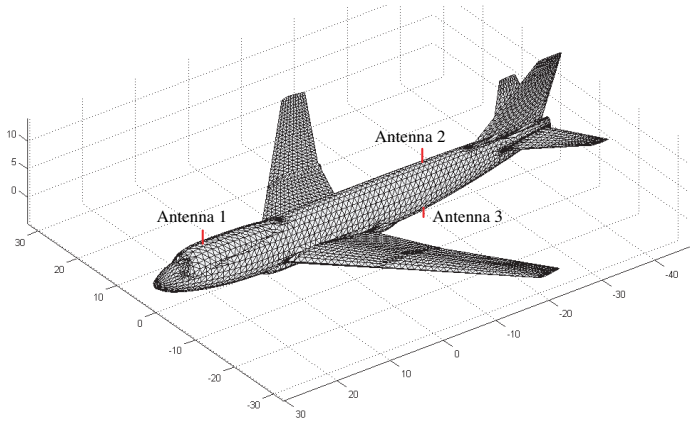

Figure 8. Three airborne monopole antennas.

All the antennas are joint-fed by point generators of equal amplitudes and phases. Fig. 9 shows the computed radiation pattern of the airborne antennas at 50 MHz. The 3D pattern is symmetrical with regard to xoz-plane due to the fact that all the antennas are mounted on the axis of the aircraft.

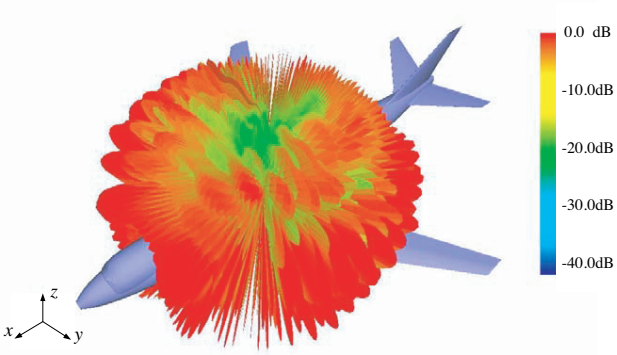

Figure 9. Normalized radiation pattern of airborne antennas.

Figure 10 shows the computed isolation between airborne antennas over a frequency range of 30 MHz∼70 MHz. We regard that $I_A > 30$ dB is the good isolation condition. From Fig. 10, it can be seen that the isolation between antennas 3 and 1 and between antennas 3 and 2 are high (low coupling) due to the shielding afforded by both fuselage and wings. The isolation between antennas 2 and 1 is much less since both antennas have line of sight of each other. For shielding absent the isolation curve of antennas 2 and 1 is relatively smooth as expected.

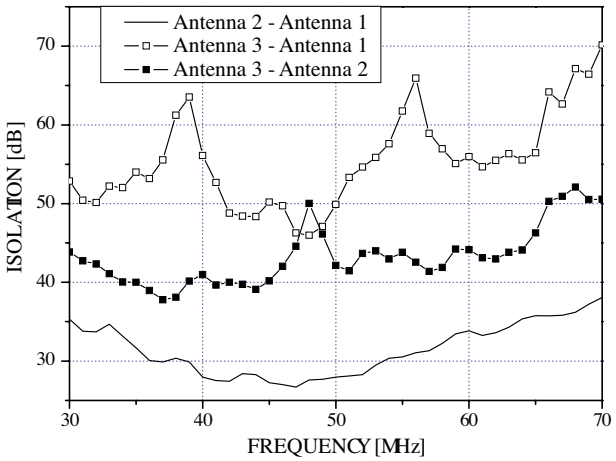

Figure 10. Isolation between airborne antennas.

4.3. Example III: Shipborne Monopole Antennas

Finally, the EMC characteristics of multiple antennas mounted on a ship model are analyzed. The model is 153 m in length and 16.5 m in width. Three thin-wire monopole antennas are positioned on the model as shown in Fig. 11.

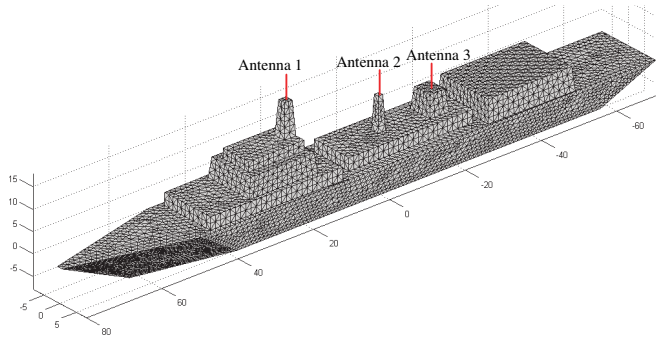

Figure 11. Three shipborne monopole antennas.

Each monopole is 2.5 m in length. The surface of the ship is represented by 12276 planar triangles (about 10 edges/wavelength at 40 MHz), and each antenna is divided into 12 segments. The center frequency of the antennas is 30 MHz, and the sweeping frequency range is 20 MHz∼60 MHz (41 sampling points).

All the antennas are joint-fed by point generators of equal amplitudes and phases. Fig. 12 shows the computed radiation pattern of the shipborne antennas at 30 MHz. Antennas 1 and 3 are mounted on the axis of the ship, while antenna 2 offsets the axis. Therefore the 3D pattern is not symmetrical with regard to *xoz*-plane.

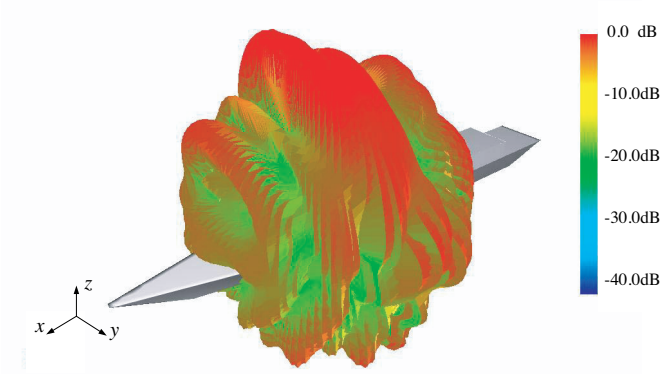

Figure 12. Normalized radiation pattern of shipborne antennas.

Figure 13 shows the computed isolation between shipborne antennas over a frequency range of 20 MHz∼60 MHz. From Fig. 13, it can be seen that antennas 2 and 1 and antennas 3 and 1 are in good isolation condition. The coupling between antennas 3 and 2 is high since the distance between the two antennas is relatively small (about 14.4 m) and both antennas have line of sight of each other.

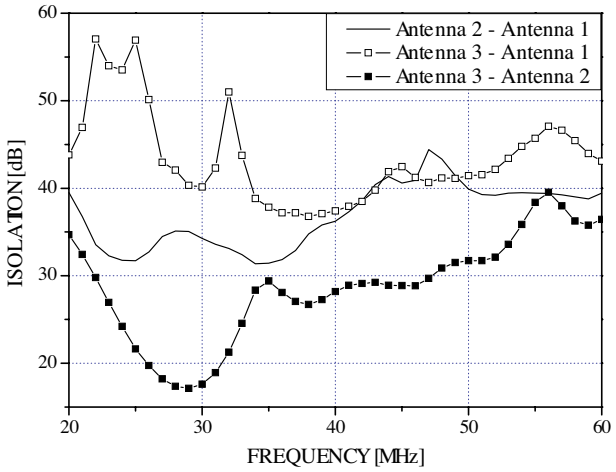

Figure 13. Isolation between shipborne antennas.

Table 1 lists the memory requirement and the CPU time for the examples shown in Fig. 8 and Fig. 11 (The convergence precision for BiCGStab ($l = 2$) is 10^{-3}). For the aircraft model, the classical MoM requires 8.3 GB memory, which is 6.2 times the maximum memory required for the MLFMA. For the ship model, the classical MoM requires 5.0 GB memory, which is 5.7 times the maximum memory required for the MLFMA. It is obvious that the MLFMA is the especially effective technique in solving large-scale EMC problems. However, the performance of the MLFMA in this paper is not necessarily the optimal, since this paper focuses on the EMC problems including multiple antennas.

Table 1. Memory requirement and CPU time for aircraft and ship models.

Model	Algorithm	Number of levels	Maximummemory (MB)	Totaltime (hr)
Aircraft	MLFMA	6∼7	1362.4	17.5
Ship	MLFMA	6∼8	902.2	20.3

5. CONCLUSION

The definition of arbitrary isolation between antennas presented in this paper is quite practical and can give the significant instructions to the actual EMC prediction. Numerical results show that the MLFMA can be the right tool for realistic EMC analysis over a wide band of frequencies. The isolation theory and the MLFMA technique in this paper will be helpful to optimize the locations of antennas on electrically large platforms, and can be extended to analyze more complex EMC problems in the real world.

ACKNOWLEDGMENT

The authors would like to thank Dr. Wei Ding and Dr. Peng Wang for helpful discussions.

REFERENCES

1. Pathak, P. H. and N. Wang, "Ray analysis of mutual coupling between antennas on a convex surface," *IEEE Trans. Antennas and Propagat.*, Vol. 29, No. 6, 911–922, 1981.
2. Liang, C. H., "New theory of isolation between antennas," *IEEE International Symposium on MAPE*, Vol. 1, 285–288, 2005.
3. Wallen, H. and J. Sarvas, "Translation procedures for broadband MLFMA," *Progress in Electromagnetics Research*, PIER 55, 47–78, 2005.
4. Wan, J. X. and C. H. Liang, "A fast analysis of scattering from microstrip antennas over a wide band," *Progress In Electromagnetics Research*, PIER 50, 187–208, 2005.
5. Wan, J. X., T. M. Xiang, and C. H. Liang, "The fast multipole algorithm for analysis of large-scale microstrip antenna arrays," *Progress In Electromagnetics Research*, PIER 49, 239–255, 2004.
6. Song, J. M., C. C. Lu, and W. C. Chew, "Multilevel fast multipole algorithm for electromagnetic scattering by large complex objects," *IEEE Trans. Antennas and Propagat.*, Vol. 45, No. 10, 1488–1493, 1997.
7. Song, J. M. and W. C. Chew, "Multilevel fast-multipole algorithm for solving combined field integral equations of electromagnetic scattering," *Microwave and Optical Technology Letters*, Vol. 10, No. 1, 14–19, 1995.

8. Chao, H. Y., "The multilevel fast multipole algorithm for electromagnetic compatibility analysis," *IEEE International Symposium on Electromagnetic Compatibility*, Vol. 2, 844–847, 1999.
9. Xie, Y., J. He, A. Sullivan, and L. Carin, "A simple preconditioner for electric-field integral equations," *Microwave and Optical Technology Letters*, Vol. 30, No. 1, 51–54, 2001.
10. Zhang, Y., Y. Xie, and C. H. Liang, "Application of the SN-preconditioning method to the integral equations for a slot-array antenna," *Microwave and Optical Technology Letters*, Vol. 37, No. 4, 302–305, 2003.
11. Zhang, Y., Y. Xie, and C. H. Liang, "A highly effective preconditioner for MoM analysis of large slot arrays," *IEEE Trans. Antennas and Propagat.*, Vol. 52, No. 5, 1379–1382, 2004.
12. Sleijpen, G. L. G. and D. R. Fokkema, "BiCGstab(ell) for linear equations involving unsymmetric matrices with complex spectrum," *Elec. Trans. Num. Analy.*, Vol. 1, 11–32, 1993.
13. Carr, M. A., M. K. Bleszynski, and J. L. Volakis, "A near-field preconditioner and its performance in conjunction with the BiCGstab(ell) solver," *IEEE Trans. Antennas and Propagat.*, Vol. 46, No. 2, 23–30, 2004.
14. Costa, M. F., "Electromagnetic radiation and scattering from a system of conducting bodies interconnected by wires," Diploma, Instituto Superir Tecnico, Lisbon, Portugal. 1976. M.S.E.E., Syracuse University, Syracuse, New York, 1979.
15. Liang, C. H., *Microwave Calculation*, 94–99, Xidian University Press, Xi'an, 1985 (in Chinese).